Involvement of Hydrogen-bonding Protons in Delocalization of the Paramagnetic Electron in a Single Crystal of Photoreduced Decatungstate

Toshihiro Yamase
Research Laboratory of Resources Utilization, Tokyo Institute of Technology, 4259 Nagatsuta, Midori-ku, Yokohama 227, Japan

Diaquahydrogen tetrakis(di-isopropylammonium) decatungstate hexahydrate, $[H_5O_2][NH_2Pr^i_2]_4[W_{10}O_{32}]\cdot 6H_2O$, has been studied in a single crystal, diamagnetically diluted by $[H_5O_2]_2[NH_2Pr^i_2]_4[W_{10}O_{32}]\cdot 4H_2O$ in a *ca.* 1 : 1 molar ratio, by means of *X*-band e.s.r. spectroscopy at 77 K. The e.s.r. spectra show the superhyperfine interaction due to eight magnetically equivalent ^1H atoms which are hydrogen-bonding water protons bonded to terminal oxygen atoms at eight equatorial WO_6 sites. There is no observable ^{183}W hyperfine interaction. The e.s.r. tensors are $g_1 = 1.840 \pm 0.001$, $g_2 = 1.838 \pm 0.001$, $g_3 = 1.831 \pm 0.001$, $A_{H_1} = (6.7 \pm 0.1) \times 10^{-4}$, $A_{H_2} = (6.2 \pm 0.1) \times 10^{-4}$, and $A_{H_3} = (4.6 \pm 0.1) \times 10^{-4}$ cm^{-1}, where each value is displaced from the tungsten–oxygen bond direction. The paramagnetic electron orbital involves the direct spin polarization of H(1*s*) orbitals and is delocalized over eight equatorial octahedra sites, through four nearly linear W–O–W bridges which link the two halves of the anion. The molecular *g* and A_H values are discussed in terms of the molecular structure. It is concluded that the semioccupied molecular orbital consists of an orbital mixing among four sets of O=W–O–W=O multiple bonds which arrange the terminal W=O groups *cis* to the nearly linear bridged moieties.

Single-crystal e.s.r. spectra of u.v.-irradiated alkylammonium polyoxomolybdates at room temperature show the formation of a localized $Mo^VO_5(OH)$ site, resulting from transfer of a hydrogen-bonding proton from an alkylammonium nitrogen atom to a bridging oxygen atom in the anion.[1–4] The analysis of e.s.r. parameters indicates the direct spin polarization between the paramagnetic electron orbital of molybdenum and the hydrogen orbital. From the direction of the maximum principal value of the ^1H superhyperfine tensor, the paramagnetic site in the anion has been determined in correlation with the *X*-ray crystal structure data. In the case of $[NH_3Me]_8[Mo_8O_{26}(MoO_4)_2]\cdot 2H_2O$, for example, $[Mo_8O_{26}(MoO_4)_2]^{8-}$ suffers from the multi-electron (up to four-electron) reduction which is four separate and independent one-electron reductions.[4] On the other hand, a preliminary single-crystal e.s.r. study of the photoreduced decatungstate $[NH_2Pr^i_2]_4[W_{10}H_{1.5}O_{32}]\cdot 8H_2O$ gives an indication that the paramagnetic electron interacts with eight equivalent protons with a large degree of delocalization.[5] The e.s.r. spectra of the photoreduced decatungstate have been measured also in frozen solutions. Photolysis of $[NBu_4]_4[W_{10}O_{32}]$ in CH_3CN gave rise to an isotropic signal ($g = 1.84$, peak-to-peak linewidth 20 G at 77 K; G = 10^{-4}T) due to formation of $[W_{10}O_{32}]^{5-}$.[6] In dimethylformamide (dmf) however the signal differs; $[W_{10}O_{32}]^{5-}$ exhibits an orthorhombic signal ($g_1 = 1.848$, $g_2 = 1.842$, and $g_3 = 1.830$ at 20 K) with a shoulder (tentatively assigned as ^{183}W hyperfine interaction line) on the low-field side.[7]

In this paper, single-crystal e.s.r. parameters of photoreduced decatungstates are discussed in connection with structural aspects governing electron spin delocalization, since details of the crystal structure of $[NH_2Pr^i_2]_2[W_{10}H_{1.5}O_{32}]\cdot 8H_2O$ have become available.[8]

Experimental

Single crystals of photoreduced decatungstate were prepared by u.v. photolysis of tetrakis(di-isopropylammonium) decatungstate–acetonitrile (1/2), $[NH_2Pr^i_2]_4[W_{10}O_{32}]\cdot 2CH_3CN$, in H_2O–CH_3CN. The oxidized form, $[NH_2Pr^i_2]_4[W_{10}O_{32}]$, was prepared by adding an aqueous solution (20 cm^3) of 2 mol dm^{-3} $[NH_2Pr^i_2]ClO_4$ to a solution of $Na_2WO_4\cdot 2H_2O$ (3 g) in water (50 cm^3), adjusted to pH 2 with $HClO_4$. The resulting yellow precipitate was dissolved by addition of CH_3CN (200 cm^3). Cooling the yellow solution yielded crystals of $[NH_2Pr^i_2]_4[W_{10}O_{32}]\cdot 2CH_3CN$ which were filtered off and dried in air [space group $P2_1/n$, with $a = 14.617(2)$, $b = 17.783(3)$, $c = 11.755(2)$ Å, $\beta = 100.27(2)°$, and $Z = 2$[8]]; i.r. (cm^{-1}) bands at 970 (sh), 950s, 890m, 790vs, 580vw, 438m, 420w, 400m, and 330w.

The reduced form was prepared by u.v. ($\lambda > 310$ nm) photolysis of $[NH_2Pr^i_2]_4[W_{10}O_{32}]\cdot 2CH_3CN$ saturated in deaerated H_2O–CH_3CN (1:19–1:4, v/v) according to a previous procedure.[6] Blue crystals of the reduced product were precipitated during the photolysis and separated by hand picking. Analysis of W^V in the blue crystals was achieved by titration with $KMnO_4$ under an atmosphere of nitrogen and indicated a composition with about 1.5-electron reduction. The *ca.* 1.5-electron reduction was confirmed by the absorption spectrum of the blue product dissolved in deaerated H_2O (pH 2)–CH_3CN (9:1, v/v), as shown in Figure 1. The observation of a band at 965 nm due to an intervalence transition and the lack of a characteristic charge-transfer band at 323 nm of the fully oxidized species indicate that the solution contains the reduced species only.[6] Colorimetric analysis of the solution using $\varepsilon_{780} = 1.1 \times 10^4$ and $\varepsilon_{630} = 1.8 \times 10^4$ dm^3 mol^{-1} cm^{-1} for the one- and two-electron reduced species respectively[6] exhibits the coexistence of both reduced species in a *ca.* 1 : 1 molar ratio.* The admission of oxygen into the blue solution resulted in a perfect restoration of the oxidized species. *X*-Ray structural analysis of the blue crystal provided the composition $[NH_2Pr^i_2]_4[W_{10}H_xO_{32}]\cdot 8H_2O$ which crystallizes in the monoclinic space group $P2_1/n$, with $a = 15.902(3)$, $b = 12.233(2)$, $c = 15.673(4)$ Å, $\beta = 93.76(2)°$, and $Z = 2$.[8],† In conjunction with the conclusion that the photolysis of $[W_{10}O_{32}]^{4-}$ in CH_3CN yielded the protonated one- and two-electron reduced species,[6]

* Absorption coefficients at 780 and 630 nm for the one- and two-electron reduced species are assumed to be the same as those obtained in CH_3CN.[6]

† The lattice constants reported in ref. 5 should be corrected for an error made in the choice of unit cell.

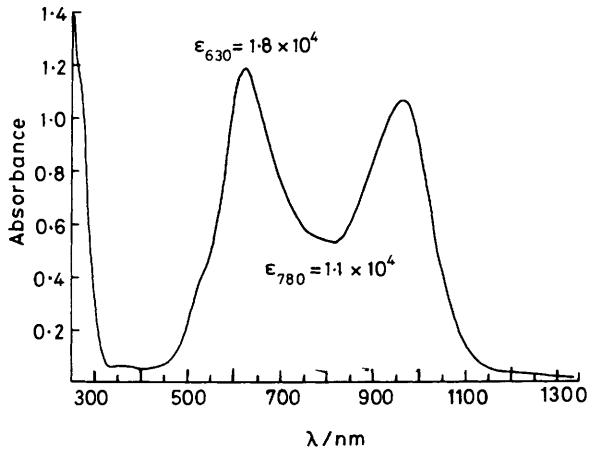

Figure 1. Electronic spectrum of $[NH_2Pr^i_2]_4[W_{10}H_{1.5}O_{32}]\cdot 8H_2O$ in deaerated H_2O (pH 2)–CH_3CN (9:1, v/v). Absorption coefficients (ε_{780} and ε_{630}) for the one- and two-electron reduced species are given in dm^3 mol^{-1} cm^{-1}

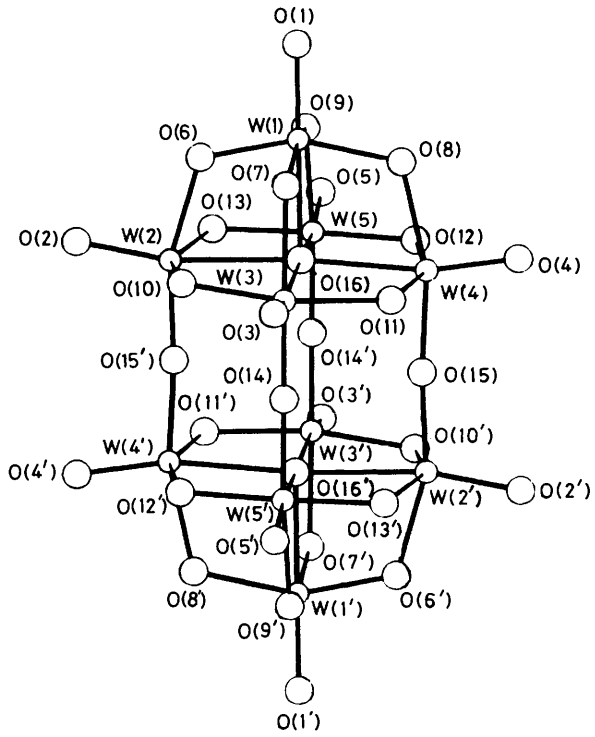

Figure 2. Structure of the photoreduced decatungstate anion $[W_{10}H_{1.5}O_{32}]^{4-}$ with atomic labelling scheme. Primed atoms are related to corresponding unprimed ones by an inversion centre

the blue crystal was therefore identified as $[NH_2Pr^i_2]_4[W_{10}H_{1.5}O_{32}]\cdot 8H_2O$, a randomly distributed equivalent mixture of $[NH_2Pr^i_2]_4[W_{10}HO_{32}]\cdot 8H_2O$ and $[NH_2Pr^i_2]_4[W_{10}H_2O_{32}]\cdot 8H_2O$ {Found: C, 9.80; H, 2.60; N, 1.95; Calc. for $[NH_2Pr^i_2]_4[W_{10}H_{1.5}O_{32}]\cdot 8H_2O$: C, 9.90; H, 2.20; N, 1.95%}; i.r. (cm^{-1}) bands at 970 (sh), 950vs, 900 (sh), 790s, 760 (sh), 720w, 620w, 540m, 500w, 440 (sh), 420 (sh), 405m, 375m, 350 (sh), and 330 (sh). Crystal structural data concerning hydrogen-bonded water molecules show that $[NH_2Pr^i_2]_4[W_{10}H_{1.5}O_{32}]\cdot 8H_2O$ can be formulated as $[H_5O_2][NH_2Pr^i_2]_4[W_{10}O_{32}]\cdot 6H_2O$ + $[H_5O_2]_2[NH_2Pr^i_2]_4[W_{10}O_{32}]\cdot 4H_2O$, as discussed below. A perspective view of the anion with the atom labelling is shown in Figure 2. The structure of $[NH_2Pr^i_2]_4[W_{10}H_{1.5}O_{32}]\cdot 8H_2O$ possesses a centre of inversion at the central cavity in the anion.

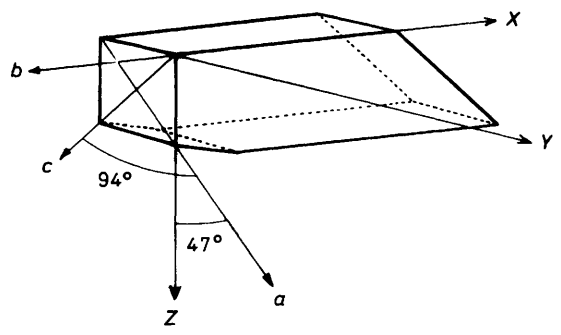

Figure 3. E.s.r. reference axes (X, Y, Z) and crystallographic directions for an idealized crystal of $[NH_2Pr^i_2]_4[W_{10}H_{1.5}O_{32}]\cdot 8H_2O$

The single crystal was mounted on a quartz rod using silicon grease. The e.s.r. spectra were recorded with a Varian E-12 X-band spectrometer equipped with accessories and measured at 77 K. In order to derive principal values of both g and ^1H superhyperfine tensors, spectra were recorded at every rotation in steps of 10° as the crystal was rotated around mutually orthogonal axes X, Y, and Z, with the axes of rotation always perpendicular to the magnetic fields H_0. The accuracy of alignment of the crystal in the e.s.r. spectrometer was checked by observing the internal consistency of the observed angular variation of the spectra. Rotation data were fitted by least squares to expressions of the type given by the diagonalization, thus giving the eigenvalues and vectors for the g and ^1H superhyperfine tensors as reported previously.[1-4] The X axis was chosen to coincide with the b direction, the Z axis being in the bisector of aOc. The morphology of the blue crystal used in the e.s.r. study is shown in Figure 3, as well as the orientation of the crystal axes determined with a Weissenberg camera. Electronic spectra were recorded with a Hitachi 330 spectrophotometer. Infrared spectra were recorded in KBr pellets with a Jasco IRA-2 spectrometer.

Results

Figure 4(a) shows an example of the e.s.r. spectrum of W^V for the magnetic field in the YZ plane. Using higher amplification nine components of equally spaced lines are observed. The peak-to-peak linewidth is *ca.* 5 G in every direction of the magnetic field. It can be concluded that the spectrum results from superhyperfine coupling with eight magnetically equivalent ^1H ($I = \frac{1}{2}$) atoms, giving a nonet of relative intensities 1:8:28:56:70:56:28:8:1. The spectra in every direction exhibit no resolution of a hyperfine structure due to the ^{183}W isotope ($I = \frac{1}{2}$) with natural abundance 14.3%. The hyperfine interaction would give small satellite doublet lines due to one ^{183}W atom only, since the low natural abundance of ^{183}W permits interaction with more than two ^{183}W atoms in the $[W_{10}H_{1.5}O_{32}]^{4-}$ anion to be neglected. Thus, the lack of hyperfine resolution must mean that the hyperfine coupling parameter is smaller than the spectrum width of *ca.* 80 G. If the magnetic field is located in the ZX plane, two paramagnetic species (A and B) are observed as shown in Figure 4(b) and the two signals coincide for the magnetic field parallel to the X axis, suggesting that the two signals arise from two magnetically non-equivalent molecules in the unit cell with $P2_1/n$ symmetry.[8] The spectrum in the ZX plane, in general, is complex due to overlapping lines of the two different molecules in the unit cell.

Table 1 summarizes the results of these measurements and Figure 5 shows the angular dependence of calculated values of

Table 1. Angular dependence of the g-value fields (H/G) and the ^{1}H superhyperfine splitting (ΔH/G) for $[NH_2Pr^i_2]_4[W_{10}H_{1.5}O_{32}]\cdot 8H_2O$ at 77 K;* ν = 9.130 GHz

Angle of rotation θ/°	*XY* plane, *X* at θ = 0°				*YZ* plane *Y* at θ = 0°		*ZX* plane, *Z* at θ = 0°			
	Species A		Species B				Species A		Species B	
	H	Δ*H*	*H*	Δ*H*	*H*	Δ*H*	*H*	Δ*H*	*H*	Δ*H*
0	3 547.6	5.3	3 547.6	5.3	3 549.4	7.1	3 561.4	7.7	3 561.2	7.7
10	3 547.5	5.2	3 548.0	5.3	3 550.0	7.0	3 562.8	7.6	3 555.8	—
20	3 547.7	5.4	3 548.4	5.7	3 551.3	7.0	3 562.5	7.3	3 554.3	7.3
30	3 547.9	—	3 548.2	5.6	3 552.0	7.1	3 558.8	6.9	3 549.4	—
40	3 548.1	6.2	3 548.6	6.3	3 553.0	7.3	3 557.6	6.6	3 547.9	6.3
50	3 548.5	6.4	3 548.9	6.6	3 555.0	7.5	3 555.9	6.0	3 546.6	5.9
60	3 548.9	—	3 549.3	—	3 556.8	7.6	3 552.3	5.7	3 544.9	5.6
70	3 549.1	7.1	3 549.6	7.2	3 558.6	7.7	3 550.2	5.6	3 544.6	5.5
80	3 549.2	7.1	3 549.6	7.2	3 560.5	7.8	3 548.2	5.5	3 545.6	5.3
90	3 549.2	7.1	3 549.2	—	3 561.4	7.8	3 547.6	5.3	3 547.0	5.3
100	3 549.6	7.2	3 549.3	7.0	3 561.6	7.8	3 546.0	5.3	3 552.2	5.6
110	3 549.4	7.1	3 549.2	7.0	3 561.0	7.8	3 546.9	5.6	3 554.8	6.0
120	3 549.3	7.0	3 549.1	6.9	3 560.3	7.7	3 548.1	6.0	3 557.6	6.4
130	3 549.2	—	3 548.7	—	3 558.6	7.7	3 550.5	6.3	3 560.1	—
140	3 549.1	6.7	3 548.4	6.7	3 557.1	7.6	3 553.5	6.6	3 561.9	7.0
150	3 548.9	6.6	3 548.2	6.5	3 555.7	7.4	3 555.8	—	3 563.0	7.5
160	3 548.4	6.4	3 547.8	6.2	3 553.4	7.3	3 558.4	7.3	3 561.6	7.6
170	3 548.0	6.0	3 547.6	5.9	3 551.8	7.2	3 560.4	—	3 561.0	7.7

* Data are reliable to ±0.1 G.

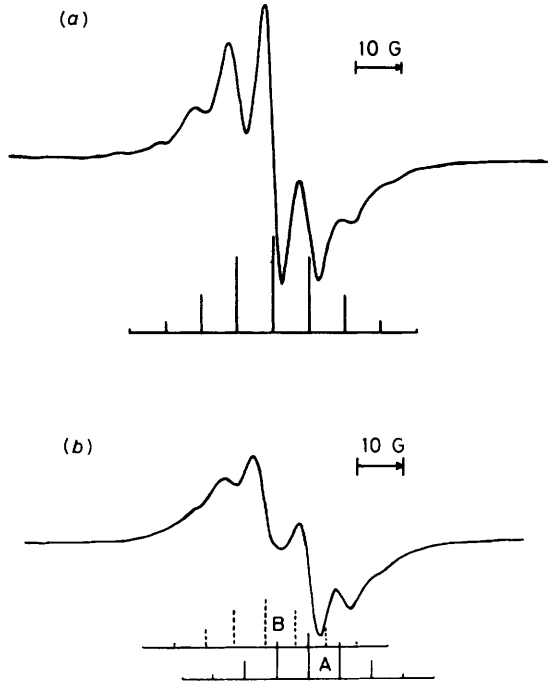

Figure 4. E.s.r. spectra of $[NH_2Pr^i_2]_4[W_{10}H_{1.5}O_{32}]\cdot 8H_2O$ at 77 K. (*a*) H_0 is in the *YZ* plane making 120° with the *Y* axis, (*b*) H_0 is in the *ZX* plane making 40° with the *Z* axis. A and B correspond to the two magnetically non-equivalent molecules in the unit cell

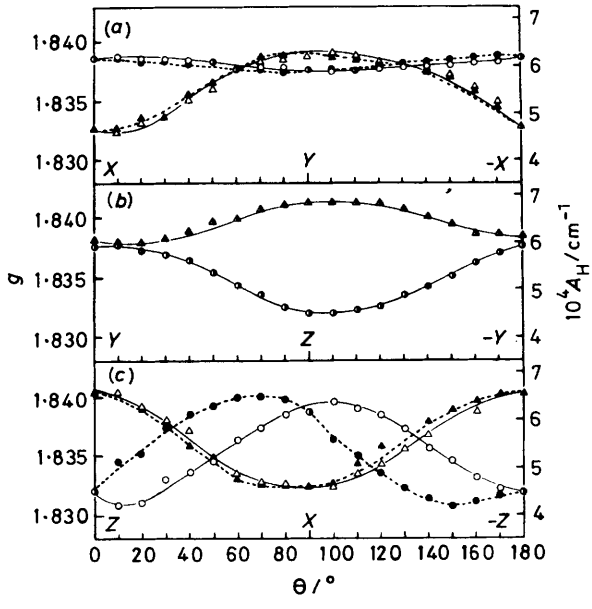

Figure 5. Angular dependence of the signals A (——) and B (– – – –) in the (*a*) *XY*, (*b*) *YZ*, and (*c*) *ZX* planes: g (○ and ● for A and B respectively) and A_H (△ and ▲ for A and B respectively)

g and ^{1}H superhyperfine splitting. For some orientations, calculation of the ^{1}H superhyperfine splittings has not been tried since the two crystallographically independent molecules make the resolution of the signal lines difficult. In the *ZX* rotation plane maximum g values ($g_{max.}$) are located. The angle between the directions of $g_{max.}$ for A and B is *ca.* 30°. This is larger than the angle (14°) between the W(1)···W(1′) [or O(16)···O(16′)] molecular axes of the two molecules projected on the *ZX* plane, suggesting a displacement of the direction of the largest value (g_1) of the g tensor from the W(1)···W(1′) or O(16)···O(16′) axis. Figure 6 shows the geometries of the two crystallographically independent molecules viewed down the *Y* axis together with the angle between the W(1)···W(1′) directions.

The spectra are interpreted using the spin Hamiltonian (1),[1]

$$\mathcal{H} = \beta H\cdot g\cdot S + \sum_H I_H\cdot A_H\cdot S \qquad (1)$$

Table 2. Electron spin resonance parameters for the two magnetically non-equivalent molecules A and B

	Principal values		Direction cosines with respect to X	Y	Z	Principal values		Direction cosines with respect to X	Y	Z
Molecule A						Molecule B				
g^a	g_1	1.839	0.9856	0.0686	−0.1545	g_1	1.840	0.8701	0.2135	0.4442
	g_2	1.838	−0.0577	0.9956	0.0740	g_2	1.837	−0.2497	0.9681	0.0239
	g_3	1.831	0.1588	−0.0642	0.9852	g_3	1.831	0.4250	0.1314	−0.8956
	g_0	1.836				g_0	1.836			
$A_H{}^b$	A_{H1}	6.7	0.0895	0.0851	−0.9923	A_{H1}	6.8	−0.1369	−0.1416	0.9804
	A_{H2}	6.2	−0.2515	0.9660	0.0602	A_{H2}	6.3	0.2500	−0.9626	−0.1041
	A_{H3}	4.6	0.9637	0.2442	0.1079	A_{H3}	4.6	0.9585	0.2309	0.1672
	A_{H0}	5.8				A_{H0}	5.9			

[a] Error ±0.001; $g_0 = (g_1 + g_2 + g_3)/3$. [b] In 10^{-4} cm^{-1}; error ±0.1 × 10^{-4} cm^{-1}; $A_{H0} = (A_{H1} + A_{H2} + A_{H3})/3$.

Table 3. Angles (°) between the g and A_H tensors for the two magnetically non-equivalent molecules A and B*

	Molecule A			Molecule B		
	A_{H1}	A_{H2}	A_{H3}	A_{H1}	A_{H2}	A_{H3}
g_1	76	101	18	73	92	17
g_2	90	11	79	82	5	89
g_3	14	88	104	163	86	73

* Angles are reliable to ±1°.

with $S = \frac{1}{2}$ and $I_H = \frac{1}{2}$. The second term represents the energy due to the superhyperfine splitting. Table 2 lists the principal values of the g and A_H tensors for the two magnetically non-equivalent molecules A and B, which exhibit the same set of principal values within experimental error. The g tensors are slightly axial but almost isotropic compared with the values ($g_1 = 1.848$, $g_2 = 1.842$, and $g_3 = 1.830$) obtained for a frozen dmf solution at 20 K.[7] The average value of the g tensor is in satisfactory agreement with the isotropic value (1.84) determined in a frozen CH_3CN solution at 77 K.[6] The peak-to-peak linewidth in the frozen solution is 20 G and too broad for isotropic ^{1}H superhyperfine interaction ($A_{H0} = 5.8$ G) to be observed. E.s.r. spectra, recorded at 5—77 K on frozen solutions in CH_3CN, consist of an almost single isotropic line at $g = 1.84$ with a linewidth of 20 G. The choice of signs given in Table 2 for the components of the A_H tensors will be discussed below. Table 3 gives angles between the g and ^{1}H superhyperfine eigenvectors. Although there are significant differences between the orientations of the molecular g and A_H tensors, there is close agreement in their values, being (between g_1 and A_{H3}, g_2 and A_{H2}, and g_3 and A_{H1}) 18° for molecule A (17° for molecule B), 11° (5°), and 14° (163°), respectively.

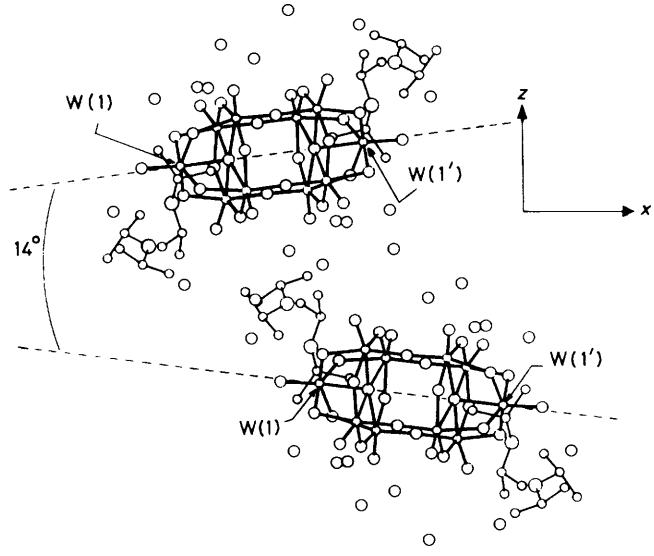

Figure 6. Geometries of the two crystallographically independent molecules viewed down the Y axis together with the angle between the W(1)···W(1') directions. Molecules at the top and bottom are assigned to A and B, respectively [alternative (I) in Table 4]

Discussion

The decatungstate consists of two W_5O_{16} units, each formed by condensing five distorted edge-shared WO_6 octahedra and bonded *via* common edges to O(16); each WO_6 octahedron has one terminal oxygen atom (Figure 2).[8,9] The cations and water molecules serve to bind the molecules together by a complex system of ionic and hydrogen bonds. Although the hydrogen atoms could not be located directly in the three-dimensional X-ray diffraction work, O···O or N···O distances in the range 2.4—3.1 Å are generally considered to involve the hydrogen-bonding proton if one hydrogen atom can be assigned to each short distance.[1,3,4] The postulated hydrogen-bonding scheme for one of the W_5O_{16} units of the molecule is illustrated in Figure 7 where the scheme is viewed in projection along the a axis. Water molecules with oxygen atoms $O_w(40)$, $O_w(30)$ or $O_w(10)$, $O_w(11)$, and $O_w(20)$ donate a hydrogen to terminal oxygen atoms at the equatorial WO_6 sites O(2), O(3), O(4), and O(5), respectively. Four O···O distances in the proposed hydrogen-bonding scheme, $O_w(40)$···O(2) [2.71(6) Å], $O_w(20)$···O(5) [2.86(4) Å], $O_w(11)$···O(4) [3.05(5) Å], and $O_w(30)$···O(3) [2.89(5) Å] involve hydrogen bonds. Water molecules with $O_w(10)$, $O_w(20)$, and $O_w(30)$ can contribute their hydrogen atoms to other water molecules also. The di-isopropylammonium N(1) and N(2) atoms, having relatively short distances [2.94(4) and 2.93(4) Å] to bridging oxygen atoms O(8) and O(9) respectively, can also contribute their hydrogen atoms to the neighbouring water oxygens $O_w(11)$ and $O_w(31)$ respectively. The $O_w(30)$···$O_w(41)$ separation [2.54(7) Å] is much shorter than the oxygen–oxygen distance in hydrogen-bonded water molecules (range 2.70—2.80 Å)[10] but seems to be slightly longer than the oxygen–oxygen separation (range 2.41—2.49 Å) in the diaquahydrogen cation $[H_5O_2]^+$.[11] Assuming that the protons in $[W_{10}H_{1.5}O_{32}]^{4-}$ belong to $[H_5O_2]^+$, the $O_w(30)$···$O_w(41)$ distance was calculated from a weighted average over two protonated species of $[W_{10}HO_{32}]^{4-}$ (one-electron) and $[W_{10}H_2O_{32}]^{4-}$ (two-electron) in a 1:1

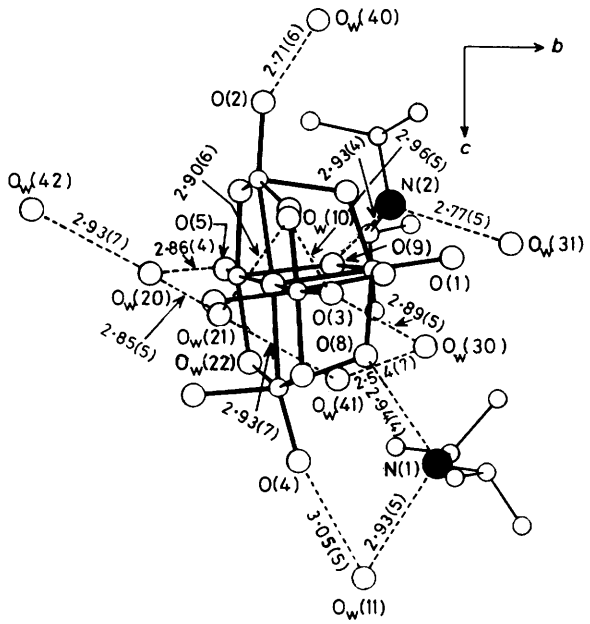

Figure 7. Plausible hydrogen-bonding scheme for a W_5O_{16} unit of the molecule. Interatomic distances are given in Å with estimated standard deviations in the least significant digits in parentheses. $O_w(11)$, $O_w(21)$–$O_w(22)$, $O_w(31)$, and $O_w(41)$–$O_w(42)$ denote $O_w(1)$, $O_w(2)$, $O_w(3)$, and $O_w(4)$ in the adjacent unit cell, which are crystallographically equivalent to $O_w(10)$, $O_w(20)$, $O_w(30)$, and $O_w(40)$, respectively

molar ratio. The calculated value [$(\sim 2.45 \times 3 + \sim 2.75)/4 \approx$ 2.53 Å] was compatible with that found in the present study. Therefore, it is possible to formulate $[NH_2Pr^i_2]_4[W_{10}H_{1.5}O_{32}]\cdot 8H_2O$ as $[H_5O_2][NH_2Pr^i_2]_4[W_{10}O_{32}]\cdot 6H_2O + [H_5O_2]_2[NH_2Pr^i_2]_4[W_{10}O_{32}]\cdot 4H_2O$. There is little difference in W–O bond distances and W–O–W angles between $[NH_2Pr^i_2]_4[W_{10}O_{32}]\cdot 2CH_3CN$ and $[NH_2Pr^i_2]_4[W_{10}H_{1.5}O_{32}]\cdot 8H_2O$ within experimental error.[8] This indicates that one- and two-electron reductions of $[W_{10}O_{32}]^{4-}$ are accompanied by little structural change in the anion, as supported by the fact that the electrochemical reduction of $[W_{10}O_{32}]^{4-}$ in CH_3CN occurred nearly reversibly for up to two-electron reduction steps.[6]

Four corner-sharing oxygen atoms O(14), O(15), O(14′), and O(15′), linking the equatorial WO_6 sites, form an empty octahedral space in combination with O(16) and O(16′) (Figures 2 and 7). Four W–O bridging bond lengths of W(2)–O(15′) [1.87(2) Å], W(3)–O(14) [1.89(2) Å], W(4)–O(15) [1.91(2) Å], and W(5)–O(14′) [1.86(2) Å] do not differ significantly and two W–O–W angles of W(2)–O(15′)–W(4′) [176(1)°] and W(5)–O(14′)–W(3′) [177(1)°] are approximately linear.[8] These distances and nearly linear angles are consistent with a significant amount of *dπ–pπ–dπ* W–O–W bonding for the four sets of W–O–W bridges, which accounts for the unique charge-transfer band of $[W_{10}O_{32}]^{4-}$ at 323 nm.[6,12] The W–O bonds [range 2.04(2)—2.13(2) Å] *trans* to these W–O–W bridging bonds are shorter than those [2.26(2)—2.38(2) Å] *trans* to the terminal W=O bonds at the equatorial sites. This disparity between the two bridging W–O distances reflects the greater *trans*-weakening influence of a more multiply bonded terminal oxygen.[13] Furthermore, the terminal W=O bond distance [range 1.67(3)—1.71(2) Å] at each equatorial site is shorter than W(1)–O(1) [1.79(2) Å],[8] suggesting that the multiplicity of the terminal W=O bond at the equatorial site is more than at the capped site.

Observation of the well resolved superhyperfine structure due to eight magnetically equivalent ^1H atoms (Figure 4) reveals that the degree of delocalization of the paramagnetic electron is large enough to interact with eight protons over several WO_6 sites in the molecule. This is in contrast with the case of the isopolyoxomolybdates consisting of edge-shared MoO_6 octahedra.[1–4] The single-crystal e.s.r. spectra revealed the formation of a localized $Mo^VO_5(OH)$ site in the anion and the electron localization on a single molybdenum site has been explained by a small degree of *dπ–pπ–dπ* Mo–O–Mo bonding, arising from the Mo–O–Mo bond angles [85.1—108.7°] departing significantly from linearity.[4] Similarly, in the W_6O_{19} structural type where all tungsten sites are equivalent and edge-shared, the paramagnetic electron remains localized on a single tungsten site, indicating that electron delocalization over edge-shared WO_6 octahedra is difficult.[14,15] Since the structure of the W_5O_{16} unit consists of edge-shared WO_6 octahedra as in the W_6O_{19} structural type, *i.e.* a WO_6-deficient W_6O_{19} lattice, therefore, the possibility of electron delocalization between equatorial and capped sites in the $W_{10}O_{32}$ lattice is unlikely and a nearly linear arrangement of the W(2)–O(16)–W(4) or W(3)–O(16)–W(5) bonds is not of π-bonding character. Thus, it is concluded that the paramagnetic electron in the $[W_{10}H_{1.5}O_{32}]^{4-}$ lattice is delocalized over eight equatorial WO_6 sites without extending to two capped WO_6 sites at 77 K and that the two-electron reduced species is diamagnetic due to a large degree of antiferromagnetic coupling of the two electrons over the equatorial WO_6 octahedra.

In connection with the plausible hydrogen-bonding proton around each terminal oxygen atom at the equatorial sites (Figure 7), the delocalization involving eight protons over the eight equatorial sites suggests an orbital mixing among four multiple bonds of O(2)=W(2)–O(15′)–W(4′)=O(4′), O(3)=W(3)–O(14)–W(5′)=O(5′), O(4)=W(4)–O(15)–W(2′)=O(2′), and O(5)=W(5)–O(14′)–W(3′)=O(3′). Table 4 shows angles between the principal *g* or A_H values and the chosen W–O bond directions. The shift of the *g* tensor from the W–O molecular directions must have its origin in an intermixing of the tungsten 5*d* orbitals caused by the low-symmetry ligand field at the distorted equatorial WO_6 sites. For alternative (I) (Table 4) the largest principal molecular *g* value (g_1) approximates to the W(1)···W(1′) or O(16)···O(16′) direction rather than any other W–O direction, as suggested by the angular variation of *g* values for two crystallographically independent molecules (Figure 6). Assuming that the alternative (I) is the correct choice, Table 5 lists angles between the principal *g* or A_H values and O···O directions in the oxygen octahedron cavity for the two crystallographically independent molecules A and B. For A and B, g_1, g_2, and g_3 approximate to O(16)···O(16′), O(14)···O(15′), and O(14)···O(15) rather than any other O···O direction, making angles of 20° for A (19° for B) 18°(7°), and 170°(22°), respectively. Figure 8 shows the orientations of molecular *g* values for alternative (I) within the oxygen O(14, 15, 14′, 15′, 16, and 16′) octahedron cavity. Although there are significant displacements of *g* eigenvectors from the O···O axes in the cavity, the approximate correspondence between the *g* and O···O axes indicates that the semioccupied molecular orbital (s.o.m.o.) consists of orbital mixing among the four sets of O=W–O–W=O multiple bonds. Accordingly, the nearly isotropic *g* tensor with a slight axiality (Table 2) reflects the nearly cubic symmetry of the oxygen octahedron cavity [O(14)···O(15), 3.20(3); O(14)···O(15′) 3.21(3); O(16)···O(16′) 3.99(4) Å; O(15)–O(14)–O(15′) 87.6(7), O(14)–O(15)–O(14′) 92.4(7), and O(16)–inversion centre–O(14) 91.4(8)°].[8] The high intensity of the electronic bands at $\lambda > 400$ nm (Figure 1) strongly supports an efficient orbital overlap arising from orbital mixing among the four sets of O=W–O–W=O multiple bonds. However a possibility of

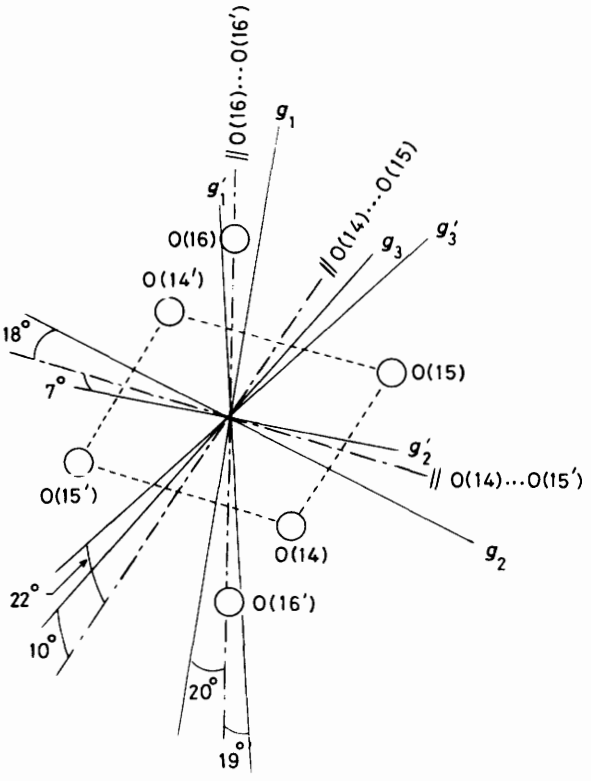

Figure 8. Orientations of molecular g values within the oxygen octahedron cavity. Unprimed and primed g values refer to molecules A and B (Figure 6), respectively (alternatives 1 and 2 in Table 5)

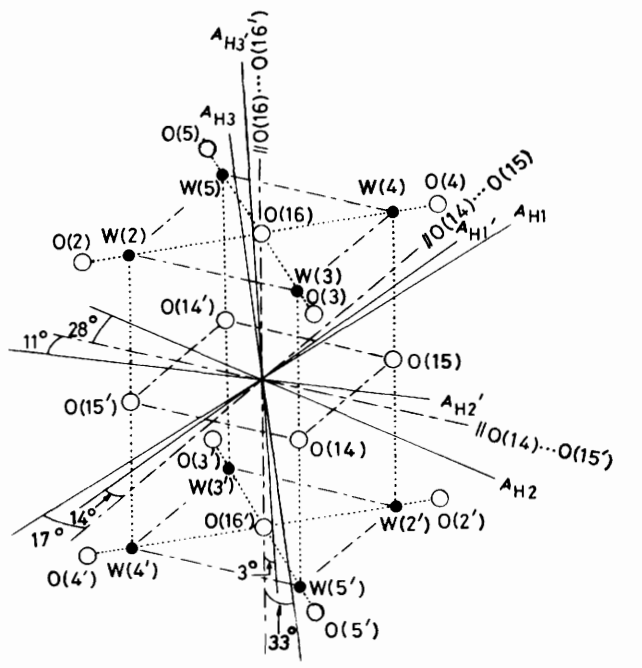

Figure 9. Orientations of molecular A_H values within the oxygen octahedron cavity. Unprimed and primed A_H values refer to molecules A and B (Figure 6), respectively (alternatives 1 and 2 in Table 5)

electronic tunnelling in the small cavity [3.20(3) × 3.21(3) × 3.99(4) Å], accounting for the delocalization of the paramagnetic electron over eight equatorial WO_6 sites, cannot be excluded.

In general, the breakdown into isotropic and anisotropic coupling constants for the components of experimental ^1H tensors gives different combinations of signs. Reasonable agreement with both sign and magnitude of the present results is obtained only using all positive signs (Table 2). The tensors are now broken up as shown below. Any other choice of signs

$$\begin{bmatrix} +6.7\,(+6.8) \\ +6.2\,(+6.3) \\ +4.6\,(+4.6) \end{bmatrix} \times 10^{-4}\ \text{cm}^{-1} = \left\{ 5.8\,(5.9) + \begin{bmatrix} +0.9\,(+0.9) \\ +0.4\,(+0.4) \\ -1.2\,(-1.3) \end{bmatrix} \right\} \times 10^{-4}\ \text{cm}^{-1}$$

results in a physically improbable anisotropic dipolar tensor. If the spin density on the tungsten atom does not contribute to spin polarization of the hydrogen bond O···H$^+$, the coupling constant for H$^+$(O) is simply related to the spin density on the oxygen atom located in a $2p$ orbital. However, spin densities estimated in this hypothesis result in unacceptably high values of either ratios (>2) of anisotropic component (B) to isotropic component (A_{iso}) or total spin count.* The large component for A_H (Table 2) indicates a direct participation of the H 1s orbital in a s.o.m.o., a situation resembling those found for the isopolyoxomolybdates.[3-5] Therefore, the maximum A_H value is expected approximately parallel to the W^V···H$^+$(O) direction at each of the eight equatorial WO_6 sites, since the direction of the maximum principal value of A_H for the isopolyoxomolybdate will lie close to the Mo^V···H$^+$(O) directions.[3-5] The observation of the eight magnetically equivalent protons (Figure 4) suggests that the protons involved in the s.o.m.o. are water protons bonded to the terminal oxygen atoms at the eight equatorial WO_6 sites, and showing similar hydrogen-bonding environments (Figure 7). If the $[NH_2Pr^i_2]^+$ protons bonded to the four bridging oxygen atoms [O(8, 9, 8', and 9')] participate in the s.o.m.o., e.s.r. spectra would show two distinguishable sets of 1:4:6:4:1 quintet superhyperfine lines due to two sets of four protons bound to four bridging and four (of eight) terminal oxygen atoms. The observable superhyperfine structure of the nonet due to the eight equivalent protons at all rotations of the magnetic field makes this hypothesis unlikely. Since the A_H values obtained would be averaged for the eight magnetically equivalent protons, the A_H tensors cannot be defined for each individual proton. However, the A_{H3} vector approximates to the O(16)···O(16') direction rather than any other O···O direction, making angles of 33° and 3° for the two crystallographically independent molecules (Table 5). In addition, the plausible W^V···H$^+$ (bonded to the terminal oxygen atom) direction at each equatorial site seems to approximate to either the O(14)···O(15) or O(14)···O(15') direction rather than the O(16)···O(16') direction (Figure 7). Considering nearly axial A_H tensors of $A_{H1} \approx A_{H2} > A_{H3}$ (Table 2), these observations suggest the correspondence of either the A_{H1} or A_{H2} vector to the plausible W^V···H$^+$(O) direction, which is in agreement with the results for the isopolyoxomolybdates. Figure 9 sketches orientations of principal axes of A_H tensors within the oxygen octahedron cavity.

A value of 0.012 (= 5.8 × 10^{-4}/474 × 10^{-4} cm^{-1} [16]) can be

* A_{H1}, A_{H2}, A_{H3} = (±6.7, ±6.2, ∓4.6), (±6.7, ∓6.2, ±4.6), and ∓6.7, ±6.2, ±4.6) × 10^{-4} cm^{-1} provide $|B|_{max.}/|A_{iso.}|$ = 2.6, 4.8, and 5.6, respectively.[16] These combinations constitute improbably high ratios. Furthermore, another combination, A_{H1}, A_{H2}, A_{H3} = (−6.7, −6.2, −4.6) × 10^{-4} cm^{-1} provides $A_{iso.}$ = −5.8 × 10^{-4} cm^{-1} which results in 0.49 of the spin density on one oxygen atom.[3] The value is unacceptably large, considering total spin density (>0.49 × 8 = 3.9) on oxygen atoms of at least eight, which would constitute atomic orbitals in the s.o.m.o. for delocalization over the eight equatorial WO_6 sites.

Table 4. Angles (°) between the principal molecular g and A_H values and the chosen molecular W–O bond directions*

	Alternative (I)						Alternative (II)					
	g_1	g_2	g_3	A_{H1}	A_{H2}	A_{H3}	g_1	g_2	g_3	A_{H1}	A_{H2}	A_{H3}
W(1)–O(1)	24	113	97	84	124	35	43	57	66	98	56	35
W(1)–O(6)	63	65	38	29	69	71	89	113	23	155	109	74
W(1)–O(7)	86	38	127	125	42	69	57	136	116	59	140	67
W(1)–O(8)	94	133	136	136	134	92	78	44	132	41	49	89
W(1)–O(9)	64	46	125	116	55	47	37	124	101	68	127	45
W(1)–O(16)	26	116	92	80	127	39	49	54	63	102	53	40
W(2)–O(2)	96	130	140	140	130	92	77	48	135	38	53	89
W(2)–O(6)	17	104	80	66	114	35	51	67	48	116	65	37
W(2)–O(10)	69	31	112	105	41	54	49	139	94	79	141	53
W(2)–O(13)	82	48	137	132	53	64	50	125	120	52	129	62
W(2)–O(15′)	21	110	96	83	122	33	42	59	65	99	58	33
W(2)–O(16)	73	58	37	32	61	79	96	122	32	152	117	82
W(3)–O(3)	67	48	130	121	56	49	37	123	106	63	126	48
W(3)–O(7)	32	122	89	77	133	46	55	48	62	104	47	46
W(3)–O(10)	76	44	49	46	47	78	92	135	45	137	131	81
W(3)–O(11)	77	74	22	16	74	87	106	108	25	167	103	91
W(3)–O(14)	19	108	95	81	120	31	42	61	63	101	60	32
W(3)–O(16)	79	40	127	122	46	61	50	132	111	62	136	59
W(4)–O(4)	65	60	41	33	64	72	89	118	28	151	114	75
W(4)–O(8)	37	123	105	93	134	44	47	46	77	88	47	43
W(4)–O(11)	79	53	140	134	58	60	45	120	120	50	124	58
W(4)–O(12)	72	30	113	107	39	56	50	140	96	77	142	55
W(4)–O(15)	21	110	92	79	122	34	45	59	61	103	58	35
W(4)–O(16)	78	56	37	34	57	83	100	125	36	150	120	86
W(5)–O(5)	83	36	125	122	42	66	55	137	112	62	141	64
W(5)–O(9)	24	106	107	93	117	28	33	63	74	89	63	27
W(5)–O(12)	74	42	52	48	46	75	89	136	46	135	132	78
W(5)–O(13)	98	111	158	160	110	89	70	68	150	18	72	85
W(5)–O(14′)	22	112	92	79	123	35	46	58	62	102	57	36
W(5)–O(16′)	74	42	127	121	49	56	45	129	108	63	133	54

* Error ±2°.

Table 5. Angles (°) between the principal molecular g and A_H values and the O···O directions in the oxygen octahedron cavity[a]

	Alternative (1)[b]						Alternative (2)[b]					
	g_1	g_2	g_3	A_{H1}	A_{H2}	A_{H3}	g_1	g_2	g_3	A_{H1}	A_{H2}	A_{H3}
O(14)···O(15)	91	80	170	163	83	75	110	81	22	166	76	93
O(14)···O(15′)	73	18	83	79	28	65	88	7	96	79	11	89
O(16)···O(16′)	20	109	93	80	121	33	19	92	71	93	92	3
O(15)···O(15′)	76	56	38	34	57	82	73	52	138	33	57	86
O(14)···O(14′)	77	40	127	122	47	60						

[a] Error ±2°. [b] Alternatives (1) and (2) correspond to the two crystallographically independent molecules A and B, respectively.

estimated for the spin population in a H 1s orbital,[3,4] which leads to a value of 0.096 (= 8 × 0.012) for the eight H(1s) contributions to the s.o.m.o. Then, a A_{H0} value for a hypothetical localized $W^{V}O_5(OH)$ site would be 47 × 10^{-4} cm^{-1} (= 8 × 5.8 × 10^{-4}). Since A_{H0} values for the localized $Mo^{V}O_5(OH)$ sites in the isopolyoxomolybdate lattices are (9.6—9.9) × 10^{-4} cm^{-1},[1-4] therefore, the proton in the hypothetical localized $W^{V}O_5(OH)$ site can be regarded as being nearly five times more strongly bound compared with the reduced isopolyoxomolybdates. It is interesting to note that the W–H bond energy for organometallic hydrides is always larger than Mo–H, subsequently giving a larger pK_a.[17]

There is no resolution of ^{183}W hyperfine structure in the e.s.r. spectra (Figure 4), while the unpaired electron localized on a single tungsten site in $[W_6O_{19}]^{3-}$ exhibits a clearly resolved signal of $A_{w\perp}$ = 74 G and $A_{w\parallel}$ = 158 G.[14] The delocalization of the paramagnetic electron over the eight equatorial WO_6 sites results in a decrease in the coupling parameter of ^{183}W ($I = \frac{1}{2}$) due to a decrease in the formal spin density on the single tungsten atom. In addition to the low natural abundance of ^{183}W (14.3%), therefore, such a decrease (probably $A_{w\perp} \approx 9$ G and $A_{w\parallel} \approx 20$ G) would make the resolution of ^{183}W hyperfine structure more difficult due to overlapping with the ^{1}H superhyperfine structure signal. This makes my calculation of the contribution of W 5d and 6s orbitals to the s.o.m.o. prohibitive.[3,4]

References

1 T. Yamase, *J. Chem. Soc., Dalton Trans.*, 1978, 283.
2 T. Yamase, R. Sasaki, and T. Ikawa, *J. Chem. Soc., Dalton Trans.*, 1981, 628.

3 T. Yamase, *J. Chem. Soc., Dalton Trans.*, 1982, 1987.
4 T. Yamase, *J. Chem. Soc., Dalton Trans.*, 1985, 2585.
5 T. Yamase, *Polyhedron*, 1986, **5**, 79.
6 T. Yamase, N. Takabayashi, and M. Kaji, *J. Chem. Soc., Dalton Trans.*, 1984, 793; N. Takabayashi and T. Yamase, *Nippon Kagaku Kaishi*, 1984, 264.
7 A. Chemseddine, C. Sanchez, J. Livage, J. P. Launay, and M. Fournier, *Inorg. Chem.*, 1984, **23**, 2609.
8 Y. Sasaki, T. Yamase, Y. Ohashi, and Y. Sasada, *Bull. Chem. Soc. Jpn.*, submitted for publication.
9 J. Fuchs, H. Hartl, W. Schiller, and U. Gerlach, *Acta Crystallogr., Sect. B*, 1976, **34**, 740.
10 C. D. Garner, N. C. Howlader, F. E. Mabbs, A. T. McPhail, and K. D. Onan, *J. Chem. Soc., Dalton Trans.*, 1979, 962 and refs. therein.
11 J. Emsley, *Chem. Soc. Rev.*, 1980, **9**, 91.
12 S. C. Termes and M. T. Pope, *Inorg. Chem.*, 1978, **17**, 500.
13 C. D. Garner, N. C. Howlader, F. E. Mabbs, A. T. McPhail, and K. D. Onan, *J. Chem. Soc., Dalton Trans.*, 1978, 1848.
14 C. Sanchez, J. Livage, J. P. Launay, and M. Fournier, *J. Am. Chem. Soc.*, 1983, **105**, 6817.
15 C. Sanchez, J. Livage, J. P. Launay, M. Fournier, and Y. Jeannin, *J. Am. Chem. Soc.*, 1982, **104**, 3194.
16 J. R. Morton, *Chem. Rev.*, 1964, **64**, 453; P. W. Atkins and M. C. R. Symons, 'The Structure of Inorganic Radicals,' Elsevier, Amsterdam, 1967, p. 24.
17 R. G. Pearson, *Chem. Rev.*, 1985, **85**, 41.

Received 11*th July* 1986; *Paper* 6/1386